Effect of different discretizations on the numerical solution of 2D aggregation population balance equation

Singh, Mehakpreet; Vuik, Kees; Kaur, Gurmeet; Bart, Hans Jörg

Important note
To cite this publication, please use the final published version (if applicable).
Please check the document version above.

Effect of different discretizations on the numerical solution of 2D aggregation population balance equation

Mehakpreet Singh *,a, Kees Vuik c, Gurmeet Kaur b, Hans-Jörg Bart d

a Department of Chemical Science, Bernal Institute, University of Limerick, Ireland
b Department of Mathematics, Indian Institute of Technology Kharagpur, Kharagpur 721302, India
c Delft Institute of Applied Mathematics, Delft University of Technology, Mekelweg 4, 2628, CD, Delft, the Netherlands
d Chair of Separation Science and Technology, University of Kaiserslautern, 67663 Kaiserslautern, Germany

ABSTRACT

This work is concerned with the assessment of the various discretizations used to obtain the numerical solutions of the bivariate aggregation population balance equation. It was illustrated in the literature that the accuracy and the efficiency of the numerical approximations is majorly controlled by the directionality and orientation of the grid selected for the domain discretization [4,6,35]. Therefore, to analyze the effect of directionality on the soution of a 2D aggregation population balance equation, four different types of discretizations have been considered and treated with a mass conserving finite volume scheme [40]. All discretizations are generated using the notion of the 'Voronoi Partitioning' and 'Delaunay Triangulation'. To examine the accuracy and efficiency of the finite volume scheme with various grids, the numerical results are compared with the exact results for several analytically tractable kernels. The comparison demonstrates that the finite volume scheme using X-type grid with logarithmic scale in the radial direction estimate different order moments as well as number density function with higher precision and efficiency as compared to the other discretizations.

© 2018 Published by Elsevier B.V.

1. Introduction

Population balances is a classical approach to describe the changes that take place in the various particulate systems. Major applications of particulate processes are in the area of pharmaceutical where sprayed fluidized bed granulator [15], twin-screw wet granulator [19] etc. are used to prepare granules. In these processes, the properties of the particles such as size, shape, porosity etc. vary due to aggregation, breakage, growth and nucleation mechanisms. In the pharmaceutical industry, multiple particle properties are required to describe the quality of the granules [16]. So, in this work, the problem related to the 2D pure aggregation population balance equation is solved. Aggregation (or agglomeration) is a complex formation mechanism in which larger sized particles are formed due to the merging of two or more smaller size particles. During this mechanism, the total number of particles decreases gradually with time but the total mass of the system remains the same.

Mathematically, the aggregation mechanism is expressed in terms of a non-linear integro-partial differential equation [14,30] which is used to track the change in number of particles in the system. During this

mechanism, the number of particles (or number density) can vary to several order of magnitude and can acquire a sharp peak. Therefore, to track the true behavior of number density, an accurate and efficient numerical scheme is required. In literature, many authors developed various numerical schemes including finite difference methods [34], finite element methods [1,3,18], monte carlo method [27–29], method of moments [42,43], least-square spectral method [9], finite volume schemes [12,17,20,33,37,40], direct quadrature method of moments [2,8,10,26,32] or sectional methods like the fixed pivot technique (FPT) [22,25,41] and cell average technique (CAT) [5,21,23,24,38].

Among all these existing techniques, sectional methods are known for their ability to predict the number distribution as well as various order moments accurately. The major disadvantage of the sectional methods is that their mathematical formulations are very complex, making the computations very expensive whereas the finite volume schemes are well known for their simple mathematical formulations. But the finite volume schemes were not able to predict the higher order moments with significant accuracy [12,33]. However, two finite volume schemes were recently developed by Singh et al. [35] and Kaur et al. [17] which not only predict the number distribution accurately but also higher order moments with some certain accuracy. Still, the accuracy of the higher order moments can be improved by choosing an appropriate discretization as shown by sectional methods when implemented on various grids [4,7,31,35]. This significantly shows that the

orientation and directionality of the grid plays significant role in predicting the various results accurately. However, the applications of the finite volume scheme are only limited to rectangular and triangular grids [36]. The triangular grid is generated by the slicing rectangular grid along the diagonal as shown in Fig. 1. Therefore, in this work, the effect of the directionality and orientation of the grids (discretizations) on the solution of a 2D PBE is analzed by treating four different discretizations with a mass conserving finite volume scheme.

The paper is ordered as follows: Section2 provides the mathematical model required to describe the 2D aggregation mechanism. Next section is used to express the idea of the generation of four different types of triangular grids and the implementation of the finite volume scheme on these grids. Further, Section4 is devoted to conduct a comparison of numerical results computed using different grids with the exact results for analytically relevant kernels. In final section, conclusions and remarks of this work are made.

2. Mathematical model

This section is used to describe the mathematical model required to track the changes takes place in the number density function ($n(x,y,t)$) as various size particles are formed in the system due to the aggregation process. Therefore, a 2D pure agglomeration population balance equation (PBE) in a well-mixed system can be written as follows:

$$\frac{\partial n(x,y,t)}{\partial t} = \underbrace{\frac{1}{2}\int_0^x \int_0^y K(x-x\prime,y-y\prime,x\prime,y\prime,t)n(x-x\prime,y-y\prime,t)n(x\prime,y\prime,t)dx\prime dy\prime}_{\text{formation of particles properties } (x,y) \text{ due to the aggregation of particles properties } (x\prime,y\prime) \text{ and } (x-x\prime,y-y\prime)}$$

$$-\underbrace{\int_0^\infty \int_0^\infty K(x,y,x\prime,y\prime,t)n(x,y,t)n(x\prime,y\prime,t)\ dx\prime dy\prime}_{\text{loss of particles properties } (x,y) \text{ due to the collision of particles properties } (x\prime,y\prime)}, \tag{1}$$

with initial data

$$n(x,y,0) = n_0(x,y),\ \ x,y \in]0,\infty[.$$

Here the aggregation kernel $K(x,y,x',y',t)$ interpret the successive collision of the two smaller size particles to build a larger size particle. Mathematical structure of the aggregation kernel is $K(x,y,x',y',t) = K_0(t)K^*(x,y,x',y',t)$ where the prefactor $K_0(t)$ describes the efficiency of the collision. Moreover, the aggregation kernel is non-negative and symmetric with respect to size variables. For the simplicity, the size dependent (or time independent) kernels are considered for this study, i.e., $K_0(t) = 1$. The most common examples of time independent kernels

are $K^*(x,y,x',y',t) = 1, x + y + x' + y', xyx'y'$. The schematic demonstration of the aggregation process is given in Fig. 2.

Since the PBE (1) is chosen to be solved with numerical method, but due to the presence of infinity in the second integral, it is very difficult to solve numerically. Hence, for the implementation of the numerical scheme, the domain must be restricted to

$$\lambda := \{(x,y) : 0 < x < x_{max}, 0 < y < y_{max}\}.$$

Therefore, the eq. (1) takes the following form

$$\frac{\partial n(x,y,t)}{\partial t} = \frac{1}{2}\int_0^x \int_0^y K(x-x',y-y',x',y',t)n(x-x',y-y',t)n(x',y',t)dx'dy'$$
$$- \int_0^{x_{max}} \int_0^{y_{max}} K(x,y,x',y',t)n(x,y,t)n(x',y',t)\ dx'dy'$$

with initial condition changes to

$$n(x,y,0) = n_0(x,y),\ \ x \in]0,x_{max}[, y \in]0,y_{max}[.$$

Further to understand the complete behavior of the system, other than number density function some integral properties namely moments of the distribution are also required [15,39]. The ijth moment of the number density function $n(x,y,t)$ is defined by

$$\mu_{ij}(t) = \int_0^\infty \int_0^\infty x^i y^j n(x,y,t)\ dxdy \tag{3}$$

Here, the zeroth order moment (μ_{00}) represents the total number of particles in the system. Whereas μ_{10} and μ_{01} expresses the total mass of the particles along the x and y axes, respectively. Moreover, the summation of μ_{10} and μ_{01} describes the total mass of the particles in the system.

3. Numerical discretizations

In this section, the mathematical formulation of the finite volume scheme on a non-uniform regular triangular grid for solving 2D aggregation PBE (2) is presented. Before providing the expressions of the numerical scheme, we first provide the brief description of the generation of four type of non-uniform regular triangular grids. The MATLAB commands voronoi and delaunayTriangulation are used to create the voronoi region and triangulation, respectively for all discretizations.
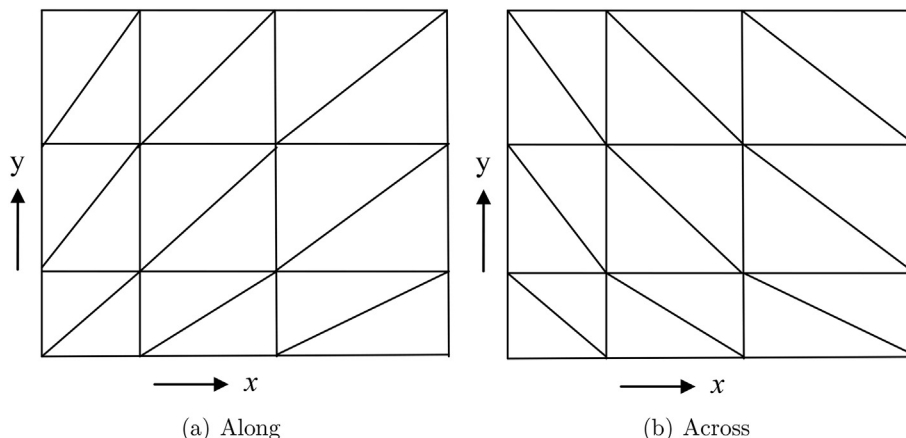

(a) Along   (b) Across

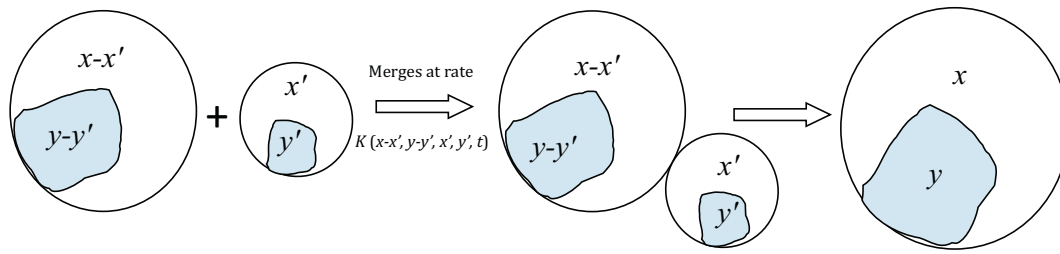**Fig. 1.** Different orientations of triangular grid.

Fig. 2. Schematic illustration of two dimensional agglomeration.

3.1. Types of domain discretizations

For generating the different grids, it is essential to fix the lower and upper bounds of the discretization domain along the horizontal axis (x-axis) and vertical axis (y-axis) as $x_{1/2} = y_{1/2} = 0$ and $]0, x_{max}]$ and $]0, y_{max}]$, respectively with $x_{max}, y_{max} < \infty$. Further, let us denote i and j as the two indices which is associated with R^{th} cell along x and y directions, respectively where $R = \{P_1, P_2, \cdots, P_I\}$ for I number of cells. The lower and upper boundaries of the Pth cell are denoted by $(x_{i-1/2}, y_{j-1/2})$ and $(x_{i+1/2}, y_{j+1/2})$, respectively, for $i = 1, 2, \ldots, I_1$ and $j = 1, 2, \ldots, I_2$. Here, the scalar values I_1, I_2 are the number of divisions of the domain in x and y directions, respectively. Therefore the total number of cells obtained are $I = I_1 \times I_2$. Corresponding to these boundaries, the 'representative' of the cell can be obtained as follows:

$$x_i = \frac{x_{i-1/2} + x_{i+1/2}}{2}, \quad y_j = \frac{y_{j-1/2} + y_{j+1/2}}{2},$$

and the length of the P th cell along m and n directions is defined as

$$\Delta x_i = x_{i+1/2} - x_{i-1/2},$$

$$\Delta y_j = y_{j+1/2} - y_{j-1/2}.$$

respectively.

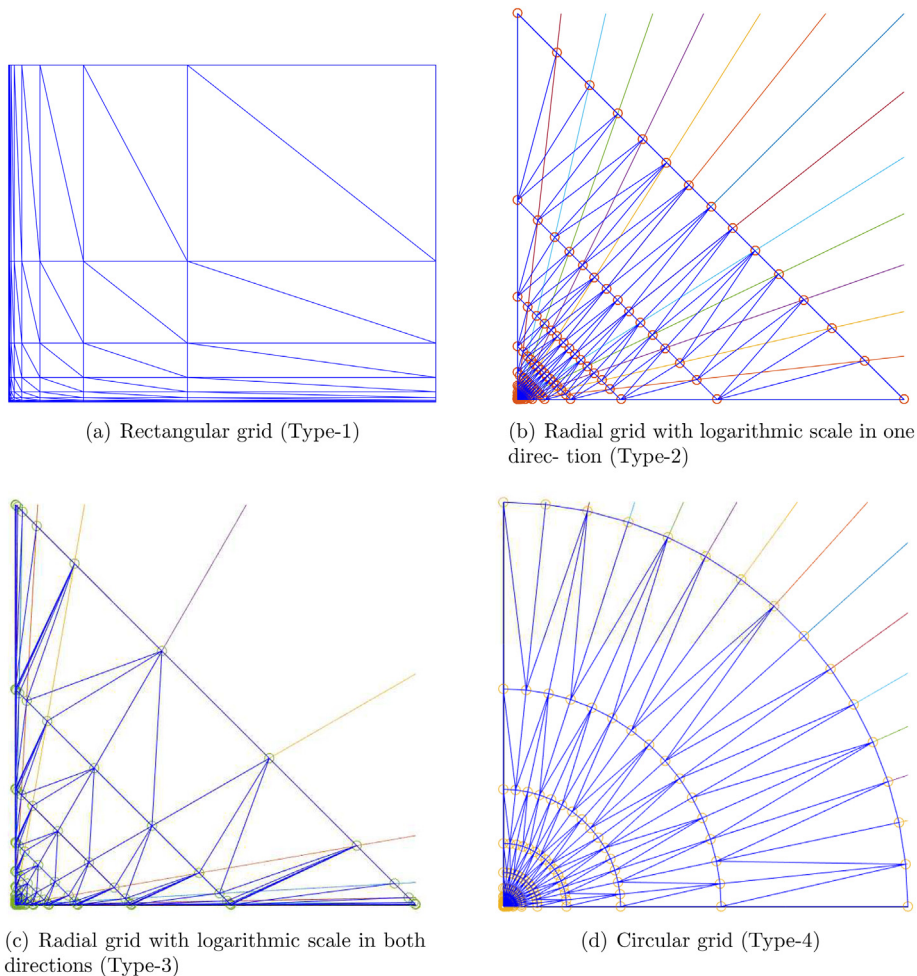(a) Rectangular grid (Type-1)

(b) Radial grid with logarithmic scale in one direc- tion (Type-2)

(c) Radial grid with logarithmic scale in both directions (Type-3)

(d) Circular grid (Type-4)

Fig. 3. Various types of domain discretizations.

Table 1
Parameters listed for simulation using size-independent kernel.

Parameters	Value
x_{min}, y_{min}	10^{-4}
x_{max}, y_{max}	20
Initial time	0
Final time	35
I_{agg}	0.97
x_{10}, y_{10}	1
N_0	1
Number of cells	15×15

3.1.1. Type-1 discretization

Draw 16 lines with exponentially increasing distance between the lines along both horizontal and vertical axes. The points at which both axes cut each other are known as grid points (lower & upper boundaries) of cells. The points on both axes are uniformly drawn on a logarithmic scale. Therefore, a larger number of grid points are obtained near the origin of the grid and decreases as we move towards the end of the grid. Further adopting these grid points, Voronoi partitioning and Delaunay triangulation is completed. We name this grid as Type-1 discretization and its representation can be seen in Fig. 3(a).
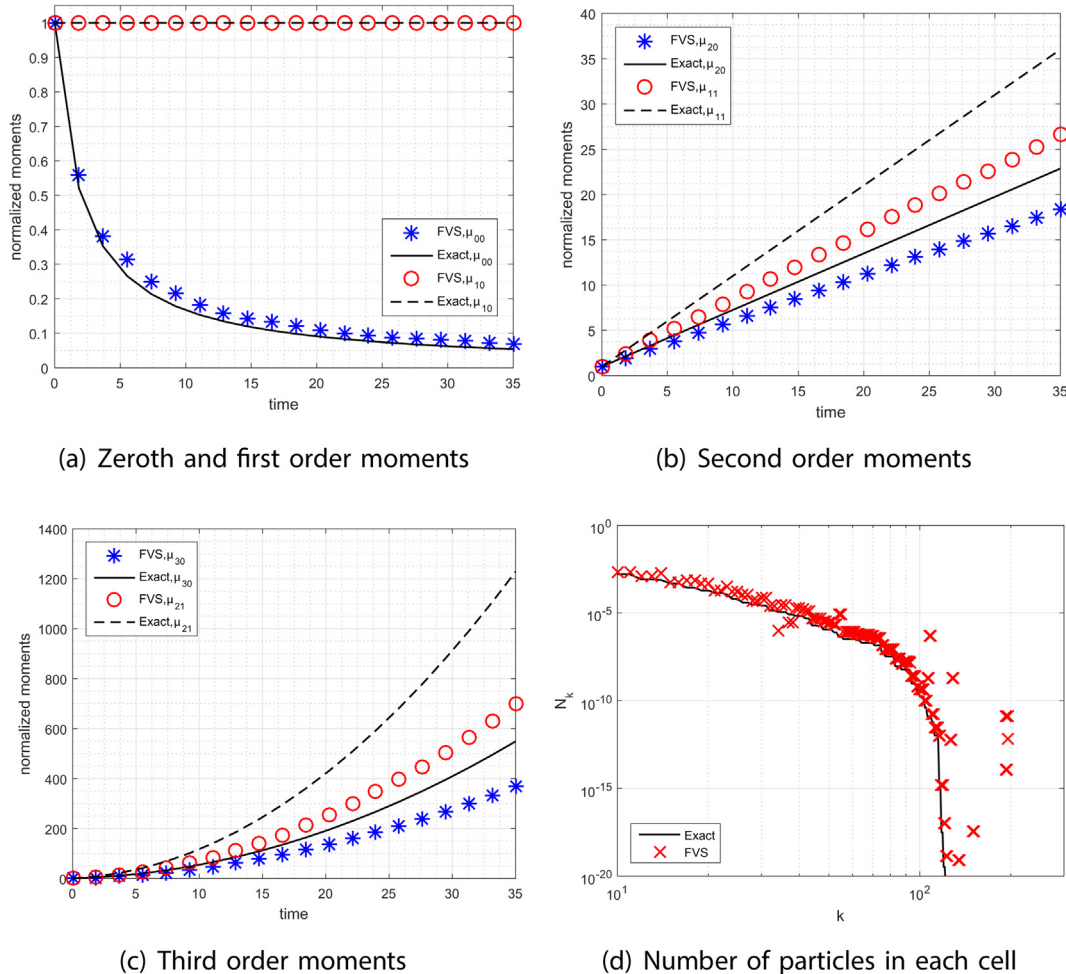
3.1.2. Type-2 discretization

This discretization is generated using two types of lines: (a) radial r-lines and (b) perpendicular t-lines are considered. The r-lines are those

lines which pass through the origin and equally partition the domain space. In our case, we have considered 16 radial lines with the angle between any two consecutive lines is $90/23 = 3.91^0$. The t-lines are the lines of slope -1. We have considered 16 t-lines for discretization. The grid points are formed when r-lines and t-lines are intersecting. The total number of pivots obtained is $15 \times 15 = 225$. Every pivot is representing some Voronoi region. Similar to the previous discretization, using these pivots, Delaunay triangulation is performed to form triangular elements. We call this discretization as Type-2 or X-type discretization. It can be noticed from the Fig. 3(b) that pivots are heavily located near the origin whereas the pivot's density reduces as we move far from the origin.

3.1.3. Type-3 Discretization

This grid is generating by modifying the previous grid (see Section 3.1.2). In contrast to the previous grid, the r-lines and t-lines are drawn on a logarithmic scale along both axes (see Fig. 3(c)). Moreover, the angles between two consecutive t-lines are considered in a way that these angles increases exponentially towards the center of the plane. This implies that the angle between lines lies near axes is smaller as compared to the angles between lines lies in the center of the grid. Whereas, the r-lines are drawn with exponentially increasing distance between the lines. In this case, 16 r-lines and 16 t-lines are considered which obtained in total 225 grid points and the points at which both lines cut each other are called pivots which are associated to some Voronoi region. Using these pivots, the triangular elements are formed. Analogous to previous grids, the more grid points are densely packed

(a) Zeroth and first order moments

(b) Second order moments

(c) Third order moments

(d) Number of particles in each cell

Fig. 4. Different order moments and number density using size-independent kernel with Type-1 discretization.

(a) Zeroth and first order moments

(b) Second order moments

(c) Third order moments
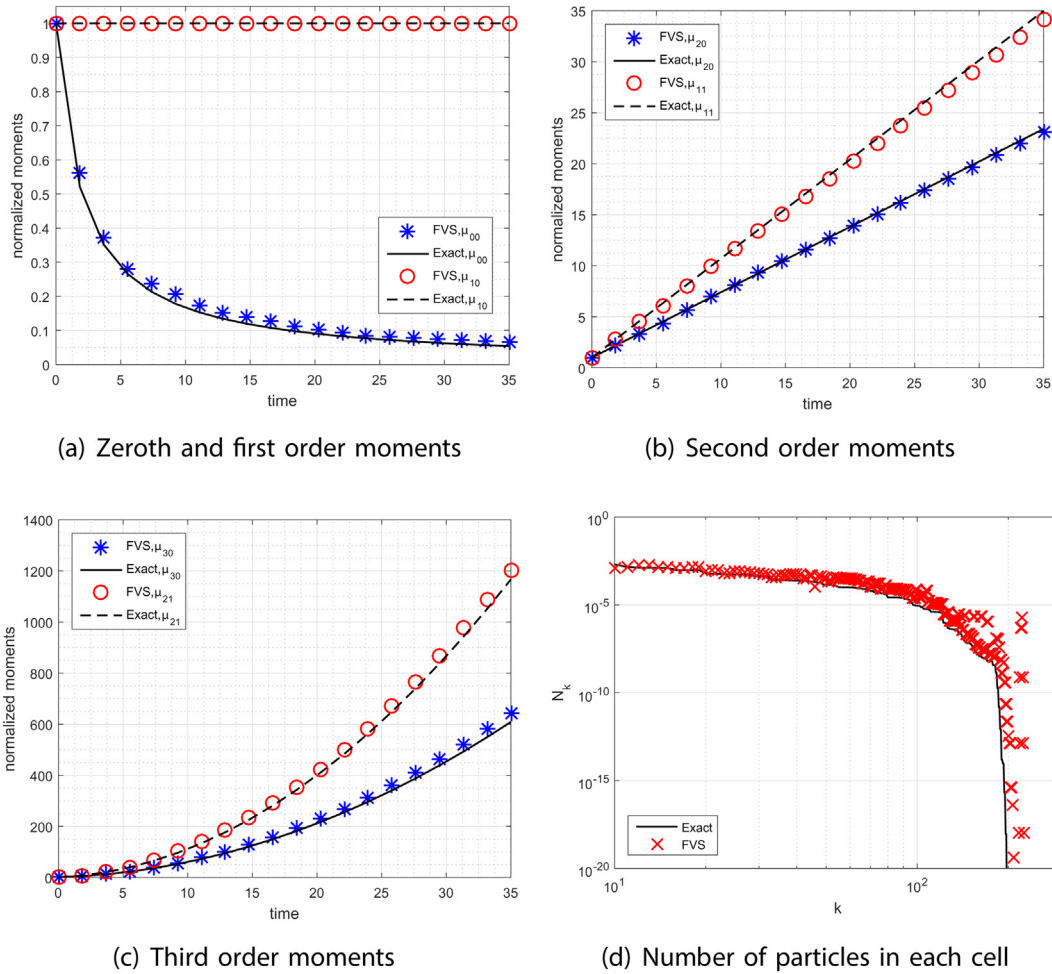

(d) Number of particles in each cell

Fig. 5. Different order moments and number density using size-independent kernel with Type-2 discretization.

near the origin of the domain and lesser at the end of the domain. We call this grid as Type-3 discretization.

3.1.4. Type-4 Discretization

This grid was first proposed by Nandanwar and Kumar [31] which consist of circular arcs (c-arcs) and radial lines (r-lines). The idea of this grid is to overcome the shortcomings due to the random orientation of triangles. To generate this grid, the radial lines are drawn in a way that the angles between any two adjacent lines remain same whereas the circular arcs are drawn in a logarithmic scale. The circular arcs are densely packed near the origin and it exponentially increases as we move far from the origin. The intersection points of these r-lines and c-arcs are considered to be the grid points. Similar to the previous cases, the formation of cells and triangles is completed. We call this grid as Type-4 discretization and can be seen in 3(b). In this work, we have considered 16 r-lines and 16 c-arcs, producing 225 pivots.

Note: Similar kind of study was also conducted by Singh et al. [35] with the cell average technique (CAT) to solve the 2D aggregation PBE. The major drawback is that the distribution of particles to neighboring pivots after the aggregation is required in the cell average technique Kumar et al. [21]. Therefore, large number of grid points are required to capture the accurate solutions of various moments and number distribution functions with these discretizations. In particular, $23 \times 25(=575)$ grid points were used to generate all four discretizations which makes the simulations computationally very

expensive. However, in our study, we only consider 225 number of cells because no distribution of particles is required for the finite volume scheme.

Now based on the aforementioned notions, let us introduce the mathematical expression of the finite volume scheme for a non-uniform regular triangular grid.

3.2. Finite volume scheme

This section is devoted to describe the mathematical formulation of the finite volume scheme developed by Singh et al. [40] for solving a bivariate aggregation PBE on a non-uniform regular triangular grid. Before describing the numerical scheme, let us presume that N_{m_p, n_q} expresses the number of particles in the cell having representatives $P = (x_i, y_j)$ which can be calculated mathematically by integrating the number density function ($n(x, y, t)$) over the boundaries of the cell, i.e.,

$$N_{x_i, y_j} = \int_{x_{i-1/2}}^{x_{i+1/2}} \int_{y_{j-1/2}}^{y_{j+1/2}} n(x, y, t) dx dy. \qquad (4)$$

Additionally, it is also assumed that the particles present within cells are concentrated on the representatives of each cell so that Dirac delta point masses can be used to approximate the number density function,
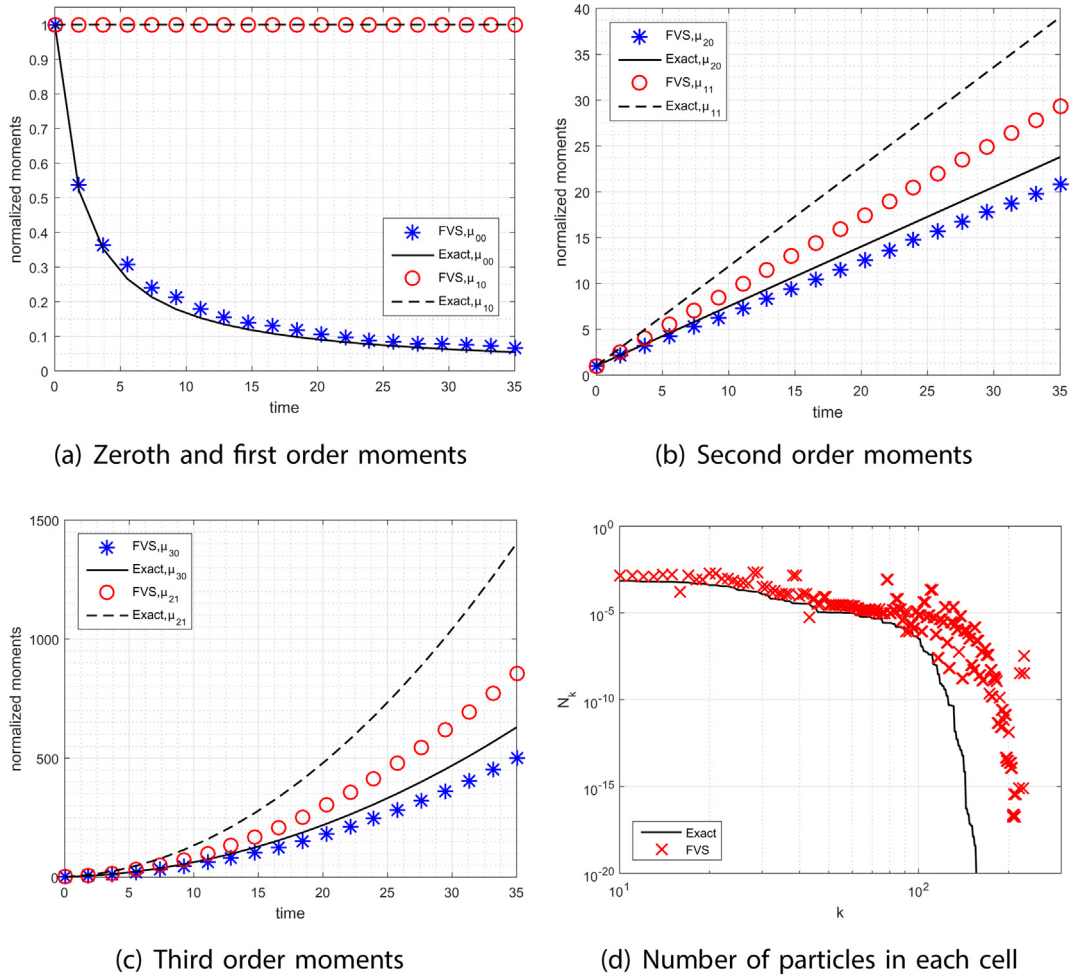
(a) Zeroth and first order moments

(b) Second order moments

(c) Third order moments

(d) Number of particles in each cell

Fig. 6. Different order moments and number density using size-independent kernel with Type-3 discretization.

i.e.,

$$n(x, y, t) = \sum_{i=1}^{I_1} \sum_{j=1}^{I_2} N_{x_i, y_j} \delta(x - x_i) \delta(y - y_j). \tag{5}$$

Substituting the Eq. (5) in the PBE (2) and integrate over the variables x and y will give the following expression:

$$\frac{dN_{x_i, y_j}}{dt} = B_{x_i, y_j} - D_{x_i, y_j}, \tag{6}$$

where the terms B_{x_i, y_j} and D_{x_i, y_j} describes the birth and death of the particles in the ijth cell, respectively and are given by

$$B_{x_i, y_j} = \sum_{\substack{p, q \\ x_{i-1/2} \leq (x_p + x_q) < x_{i+1/2}}}^{p \geq q} \sum_{\substack{r, s \\ y_{j-1/2} \leq (y_p + y_q) < y_{j+1/2}}}^{r \geq s} \left(1 - \frac{1}{2} \delta_{p,q} \delta_{r,s}\right) K_{ijkl} N_{x_p, y_r} N_{x_q, y_s}, \tag{7}$$

and

$$D_{x_i, y_j} = \sum_{p=1}^{I_1} \sum_{q=1}^{I_2} K_{ipjq} N_{x_i, y_j} N_{x_p, y_q}. \tag{8}$$

Here $K_{ijkl} = K_{x_i, y_j, x_k, y_l}$ is used for simplicity. The detailed derivation of above equations is provided in Kumar et al. [21]. Moreover, it can be observed that the formulation represented by the Eq. (6) captures the number preservation property very well, however, it does not conserve the total mass of the system which is a necessary condition for any finite volume scheme (see Appendix A). This can be easily achieved by adding a weight to the formulation (6) which yields

$$\frac{dN_{x_i, y_j}}{dt} = \sum_{(p,q,r,s) \in \Omega^{i,j}} \left(1 - \frac{1}{2} \delta_{p,q} \delta_{r,s}\right) K_{ijkl} N_{x_p, y_r} N_{x_q, y_s} \Lambda_{p,q,r,s}^{i,j}$$

$$- \sum_{p=1}^{I_1} \sum_{q=1}^{I_2} K_{ipjq} N_{x_i, y_j} N_{x_p, y_q}. \tag{9}$$

Here the weight is defined by

$$\Lambda_{p,q,r,s}^{i,j} = \begin{cases} \dfrac{x_p + x_q + y_r + y_s}{x_i + y_j}, & (p, q, r, s) \in \Omega^{i,j} \\ 0, & otherwise. \end{cases} \tag{10}$$

Here, $\Lambda_{p, q, r, s}^{i, j}$ is responsible for the conservation of the mass of the system. Moreover, $\Omega^{i,j}$ is defined as a pair of cells having representative (x_p, y_r) and (x_q, y_s) such that after the aggregation, i.e., $(x_p + x_q + y_r + y_s)$ falls in a cell having representative (x_j, y_j) and mathematically can be
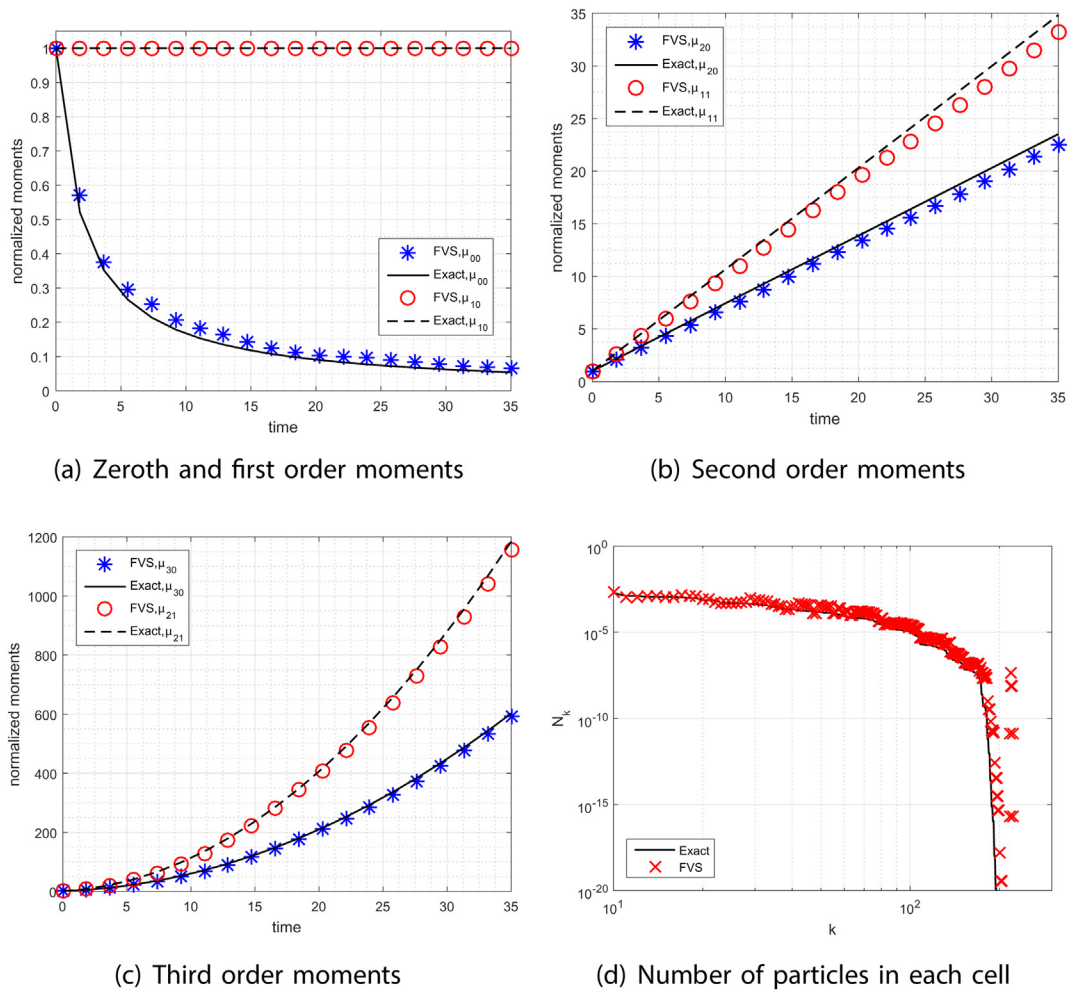
(a) Zeroth and first order moments

(b) Second order moments

(c) Third order moments

(d) Number of particles in each cell

Fig. 7. Different order moments and number density using size-independent kernel with Type-4 discretization.

Table 2
Weighted error of number distribution using size-independent kernel with various grids (15 × 15).

ψ	Type-1	Type-2	Type-3	Type-4
ψ_{00}	0.36142	0.18080	0.59055	0.24997
ψ_{10}	0.36142	0.18080	0.59055	0.24997
ψ_{20}	0.36142	0.18080	0.59055	0.24997
ψ_{11}	0.40433	0.13099	0.56943	0.14138
ψ_{21}	0.53061	0.17481	0.63632	0.18252
ψ_{30}	0.36142	0.18080	0.59055	0.24997

Table 4
Maximum error in different order moments using size-independent kernel with 15 × 15 cells.

η	Type-1	Type-2	Type-3	Type-4
η_{00}	0.12367	0.08311	0.09421	0.10974
η_{10}	3.39×10^{-07}	4.25×10^{-08}	1.32×10^{-06}	8.66×10^{-06}
η_{20}	0.17949	0.00849	0.11415	0.04764
η_{11}	0.24662	0.02071	0.24030	0.05011
η_{21}	0.41981	0.02432	0.38496	0.02721
η_{30}	0.56396	0.26336	0.35669	0.29488

Table 3
Weighted error of number distribution using size-independent kernel with various grids (30 × 30).

ψ	Type-1	Type-2	Type-3	Type-4
ψ_{00}	0.21423	0.05896	0.29523	0.13311
ψ_{10}	0.21423	0.05896	0.29523	0.13311
ψ_{20}	0.21423	0.05896	0.29523	0.13311
ψ_{11}	0.28433	0.04267	0.31763	0.06558
ψ_{21}	0.29265	0.06729	0.30897	0.08345
ψ_{30}	0.21423	0.05896	0.29523	0.13311

Table 5
Maximum error in different order moments using size-independent kernel with 30 × 30 cells.

η	Type-1	Type-2	Type-3	Type-4
η_{00}	0.08956	0.02625	0.06652	0.04595
η_{10}	2.21×10^{-11}	1.19×10^{-15}	9.16×10^{-10}	4.89×10^{-10}
η_{20}	0.09657	0.00219	0.05942	0.01324
η_{11}	0.14378	0.00932	0.13091	0.03957
η_{21}	0.23578	0.01056	0.20524	0.01591
η_{30}	0.29657	0.11978	0.21986	0.16533

Table 6
Comparison of computational time taken by FVS using size-independent kernel with various grids.

Grid Type	Time Taken (in seconds)
Type-1	3.80
Type-2	2.30
Type-3	6.97
Type-4	2.52

Table 7
Parameters listed for simulation using size-dependent kernel.

Parameters	Value
x_{min}, y_{min}	10^{-4}
x_{max}, y_{max}	120
Initial time	0
Final time	15
I_{agg}	0.80
x_{10}, y_{10}	1
N_0	1
Number of cells	15×15

Table 8
Weighted error of number distribution using size-dependent kernel with various grids with 15×15 cells.

ψ	Type-1	Type-2	Type-3	Type-4
ψ_{00}	0.11138	0.04420	0.09620	0.06021
ψ_{10}	0.11138	0.04420	0.09620	0.06021
ψ_{20}	0.11138	0.04420	0.09620	0.06021
ψ_{11}	0.43543	0.20251	0.37172	0.27187
ψ_{21}	0.64511	0.33132	0.56131	0.43829
ψ_{30}	0.11138	0.04420	0.09620	0.06021

Table 9
Weighted error of number distribution using size-dependent kernel with various grids with 30×30 cells.

ψ	Type-1	Type-2	Type-3	Type-4
ψ_{00}	0.05968	0.02086	0.04010	0.03255
ψ_{10}	0.05968	0.02086	0.04010	0.03255
ψ_{20}	0.05968	0.02086	0.04010	0.03255
ψ_{11}	0.28965	0.00908	0.19852	0.15927
ψ_{21}	0.36597	0.15369	0.30294	0.21951
ψ_{30}	0.05968	0.02086	0.04010	0.03255

expressed as

$$\Omega^{i,j} = \left\{ (p,q,r,s) \in \mathbb{N}^4 : x_{i-1/2} \leq (x_p + x_q) < x_{i+1/2} \ \& \ y_{j-1/2} \leq (y_p + y_q) < y_{j+1/2} \right\}. \tag{11}$$

Further, integrate the Eq. (9) with respect to time from limits t^k to t^{k+1}, we get the final relation for the finite volume scheme as

$$N_{x_i,y_j}^{k+1} = N_{x_i,y_j}^k + \Delta t^k \Big(\sum_{(p,q,r,s) \in \Omega^{i,j}} \Big(1 - \frac{1}{2} \delta_{p,q} \delta_{r,s} \Big) K_{ijkl}^k N_{x_p,y_r}^k N_{x_q,y_s}^k \Lambda_{p,q,r,s}^{i,j}$$

$$- \sum_{p=1}^{I_1} \sum_{q=1}^{I_2} K_{ipjq}^k N_{x_i,y_j}^k N_{x_p,y_q}^k \Big), \tag{12}$$

where $\Delta t^k = t^{k+1} - t^k$ for $k \in \{0,1,...,N-1\}$. The detailed description of the finite volume scheme and the theoretical proof of the mass

Table 10
Maximum error in different order moments using size-dependent kernel with 15×15 cells.

η	Type-1	Type-2	Type-3	Type-4
η_{00}	0.03057	0.00673	0.01922	0.01591
η_{10}	8.28×10^{-04}	9.22×10^{-05}	2.70×10^{-03}	2.36×10^{-04}
η_{20}	0.14176	0.04270	0.13675	0.09811
η_{11}	0.18723	0.05153	0.23695	0.10785
η_{21}	0.46328	0.16747	0.51941	0.30090
η_{30}	0.38329	0.27252	0.30595	0.31492

Table 11
Maximum error in different order moments using size-dependent kernel with 30×30 cells.

η	Type-1	Type-2	Type-3	Type-4
η_{00}	0.01119	0.00312	0.01032	0.01591
η_{10}	1.71×10^{-09}	3.51×10^{-11}	9.12×10^{-08}	7.45×10^{-08}
η_{20}	0.08637	0.02113	0.06589	0.04697
η_{11}	0.10915	0.02915	0.14320	0.05968
η_{21}	0.26587	0.09152	0.27611	0.16550
η_{30}	0.20310	0.14363	0.16225	0.18360

Table 12
Comparison of computational time taken by FVS using size-dependent kernel with various grids.

Grid Type	Time Taken (in seconds)
Type-1	6.97
Type-2	5.33
Type-3	5.80
Type-4	5.73

conservation property along with the CFL condition for the positivity of the solution can be found in Singh et al. [40].

4. Results and discussion

In this part of the paper, the numerical results determined using FVS with various triangular discretizations are compared with the analytical results for different analytically relevant kernels. Gelbard and Seinfeld [13] and Fernández-Díaz and Góez-García (2007) have provided the analytical solutions for size-independent and size-dependent kernels, respectively corresponding to the distinct initial conditions. For our study, the initial condition $n(x,y,0) = \frac{16N_0 xy}{x_{10}^2 y_{10}^2} \exp(-\frac{2x}{x_{10}} - \frac{2y}{y_{10}})$ is chosen for calculating the numerical as well as analytical (or exact) solutions. The comparison is conducted in terms of various order moments along with the particle population in each cell, i.e., the number density functions. Simulations are run using MATLAB on a i5 CPU with 2.40 GHz and 8 GB RAM.

Since the number density function will be 3D surface plot (i.e., $n(x,y,t)$ vs x vs y) and to see the difference between analytical and numerical solutions is very difficult in a single plot. Therefore, the concept of *flat representation* suggested by Chakraborty and Kumar [4] is used. In the flat representation, cells are sorted from $k = 1$ to $k = I_1 \times I_2$ and then the particle population in each cell is determined mathematically by $N_k = n_{k_1, k_2} \Delta x_{k_1} \Delta y_{k_2}$, is plotted against its index k. To enhance the comparison, the quantitatively weighted errors exist in the number distribution are also measured using:

$$\psi_{i,j}(t) = \frac{\sum_{k=1}^{I_1} \sum_{l=1}^{I_2} | N_{k,l}^{exc}(t) - N_{k,l}^{num}(t) | \ x_k^i y_l^j}{\sum_{k=1}^{I_1} \sum_{l=1}^{I_2} N_{k,l}^{exc}(t) x_k^i y_l^j}. \tag{13}$$

(a) Zeroth and first order moments

(b) Second order moments

(c) Third order moments
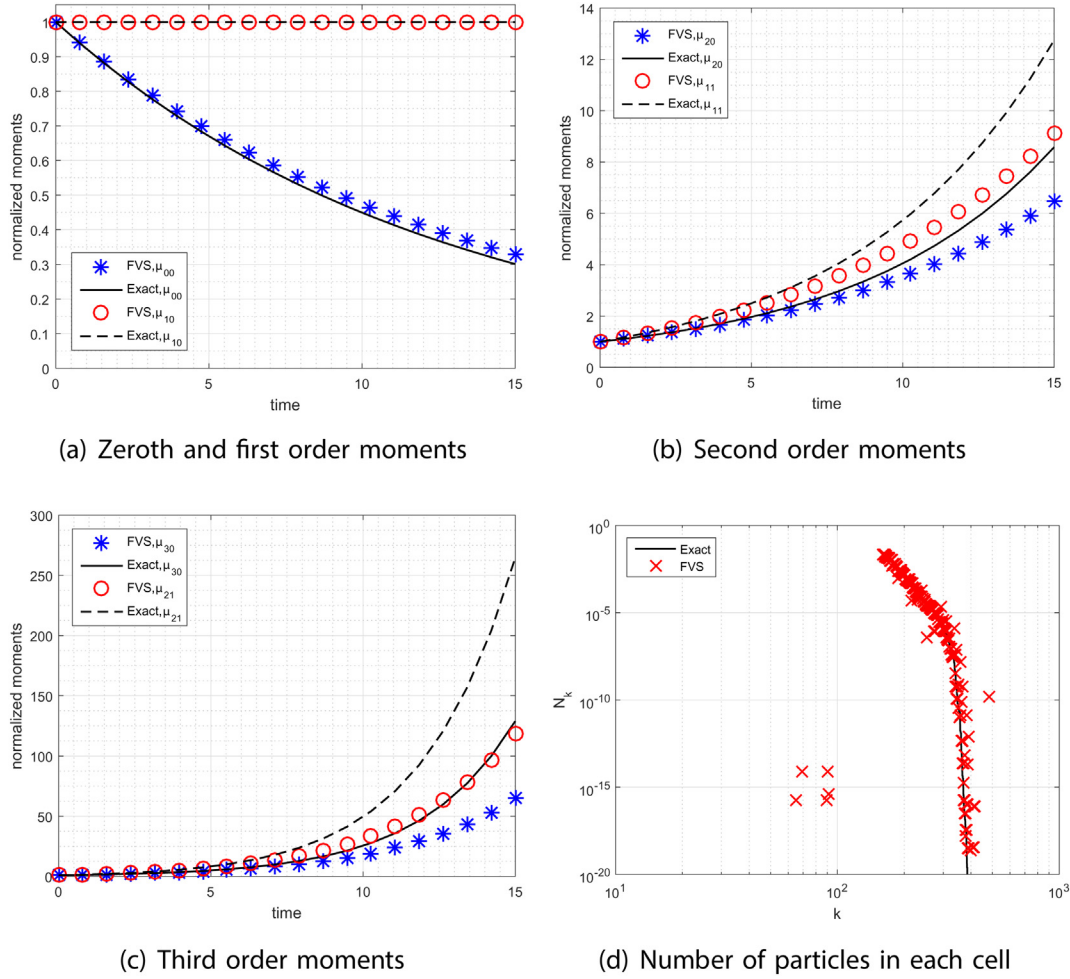

(d) Number of particles in each cell

Fig. 8. Different order moments and number density using size-dependent kernel with Type-1 discretization.

The symbols *exc* and *num* represent the exact and numerical solutions, respectively. Moreover, ψ_{00} and ψ_{10} or ψ_{01} expresses the relative error in the total number of particles (zeroth order moment) and the total mass of the system (first order moments), respectively over the whole domain. Similarly, other combinations of i and j can be computed. Additionally, the maximum error in various order moments are calculated using the mathematical expression

$$\eta_{i,j} = \max_t \left| \frac{\mu_{i,j}^{exc}(t) - \mu_{i,j}^{num}(t)}{\mu_{i,j}^{exc}(t)} \right|. \tag{14}$$

Here η_{00} and η_{10} exhibits the maximum errors in the zeroth and first order moments, respectively. These errors are evaluated at the final time.

Before interpreting the different numerical result, it is necessary to define degree of aggregation (DOA) I_{agg}:

$$I_{agg}(t) = 1 - \frac{\mu_{00}(t)}{\mu_{00}(t=0)}, \quad t \geq 0. \tag{15}$$

which describes the reduction of number of initial primary particles due to agglomeration process. Initially at $t = 0$, $I_{agg} = 0$ and as the limit t approaches ∞, I_{agg} tends to unity with all primary particles forming one aggregate.

4.1. Size-independent Kernel

Firstly, a size-independent kernel, i.e., $K(t,x,y,x',y') = K_0(t)$ is chosen to conduct the comparison of numerical and analytical results. This kernel is also well known as an constant kernel. For simplicity, the value of $K_0(t) = 1$ which physically reveals that the aggregation between two particles will always take place when they collide with each other. Other parameters required to run a simulation for a size-independent aggregation kernel are listed in Table 1. The analytical result for the number density function was derived by Gelbard and Seinfeld [13].

The quantitative comparison of various order moments and number density functions corresponding to four various discretizations are illustrated in Figs. 4, 5, 6 and 7. It can be observed that the zeroth order moments which denotes the number of particles in each cell predicted numerically show over prediction from the analytical result. This is possibly due to the fact that this numerical scheme is only focused on conserving the total mass of the system rather than preserving the zeroth order moment. Moreover, the total mass of the system, i.e., the first order moments obtained numerically using all discretization are matching well with the analytical result. In addition, the second order moments (μ_{20} & μ_{11}) computed numerically are showing a more accurate solution for Type-2 discretization than the other three discretizations. Moreover, similar kind of behavior is exhibited by the third order moments, i.e., the third order moment approximated with Type-2 discretization shows lesser deviation from the analytical moment than the other grids.
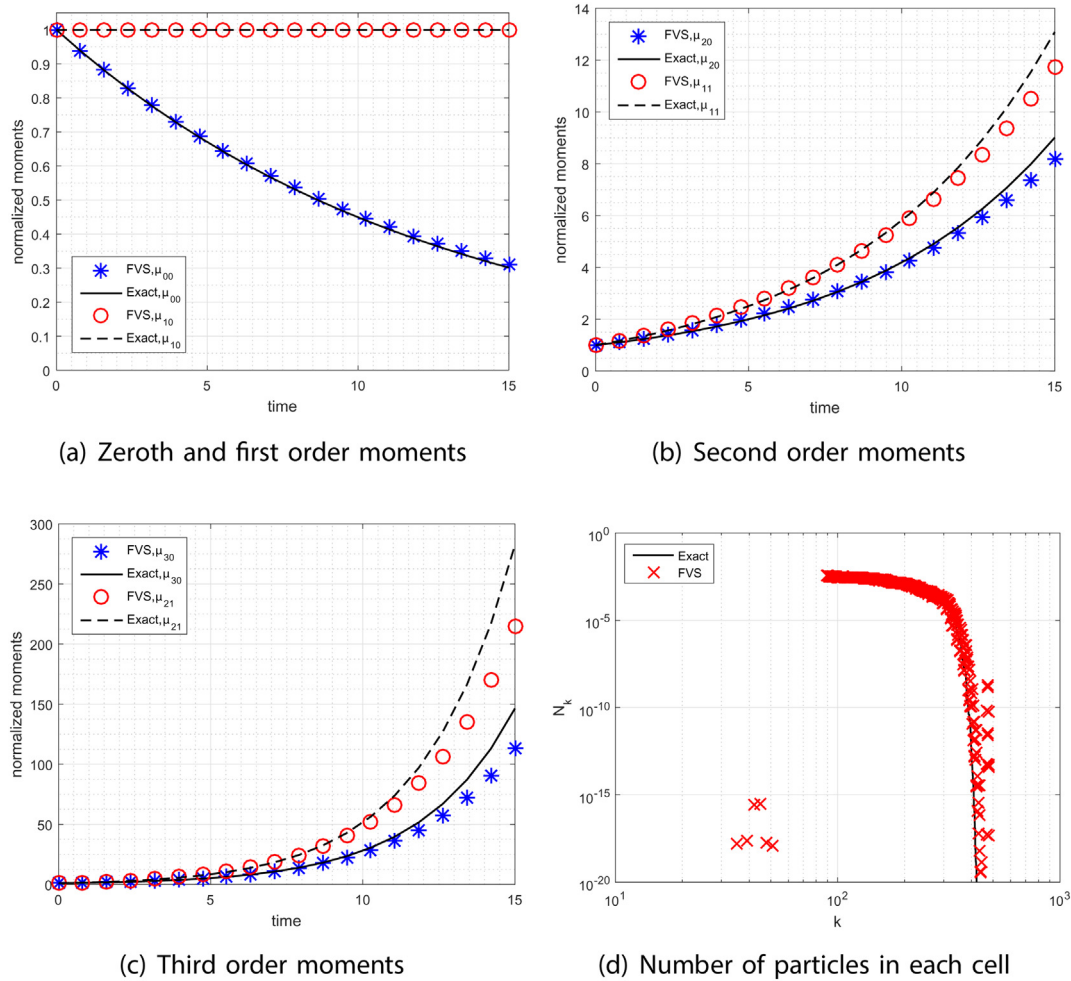
(a) Zeroth and first order moments

(b) Second order moments

(c) Third order moments

(d) Number of particles in each cell

Fig. 9. Different order moments and number density using size-dependent kernel with Type-2 discretization.

Analogous to above qualitative analysis, we have also analyzed the results related to the number density functions graphically as shown in Figs. 4(d), 5(d), 6(d) and 7(d) using the notion of flat representation for four different discretizations. The results reveal that the particle population in each cell (number density function) computed for the Type-2 discretization shows better approximation than the other grids. This same conclusion can also be made when quantitative weighted sectional errors (13) in number density functions for four discretization are calculated (see Table 2). It can be observed that the weighted sectional errors in various order moments obtained using Type-2 discretization is comparatively lesser than the other discretizations. Furthermore, the total maximum errors exist in various order moments are quantified using the expression (14) in Table 4 for four distinct discretizations. One can notice that the maximum errors in different order moments computed using Type-1, Type-3 and Type-4 are more as compared to the errors calculated using Type-2 grid. Moreover, the same comparison is also conducted using a refined grid with cell 30 × 30 as shown in Tables 3 and 5. It can be observed that the quantitative sectional and maximum errors reduced significantly for each discretizations when calculated using a refined grid. However, still Type-2 discretiztion performs better than the other discretiztions.

In order to show the efficiency of the finite volume scheme with various discretizations, the comparison of various grids is also conducted in terms of computational time, i.e.,the time taken by the finite volume scheme to obtain the various numerical results. Table 6 demonstrates that the computational time taken for computing all numerical results

by Type-2 is lesser than the other discretizations. Hence, from the above discussion, it can be easily concluded that the finite volume scheme with the Type-2 discretization computes the different results more accurately and efficiently than the other three discretizations.

4.2. Size-dependent Kernel

Similar to the previous kernel, the numerical simulations are also run for obtaining the results corresponding to the size-dependent kernel, i.e., $K(x,y,x',y',t) = K_0(t)(x + y + x' + y')$ where $K_0(t) = 1$. This is also known as an additive kernel. In contrast to the size-independent kernel, the larger size particles aggregate at a faster rate for this kernel due to higher size dependency of the kernel. The analytical result for the number density function using this complex kernel was derived by [11]. The parameters required to run the simulation for this kernel are listed in Table 7.

The numerical results for various order moments along with the number density function predicted using the finite volume scheme with four discretizations are demonstrated in Figs. 8, 9, 10 and 11. It can be observed that the zeroth order moments obtained using Type-1, Type-3 and Type-4 discretizations show over-prediction from the analytical result whereas the zeroth order moment predicted with Type-2 matches well with the analytical moment. Additionally, the first order moments for four kinds of discretizations show very good agreement with the analytical moment, i.e., the mass conservation property holds for all discretizations. Moreover, the second order moments (mu_{11} &
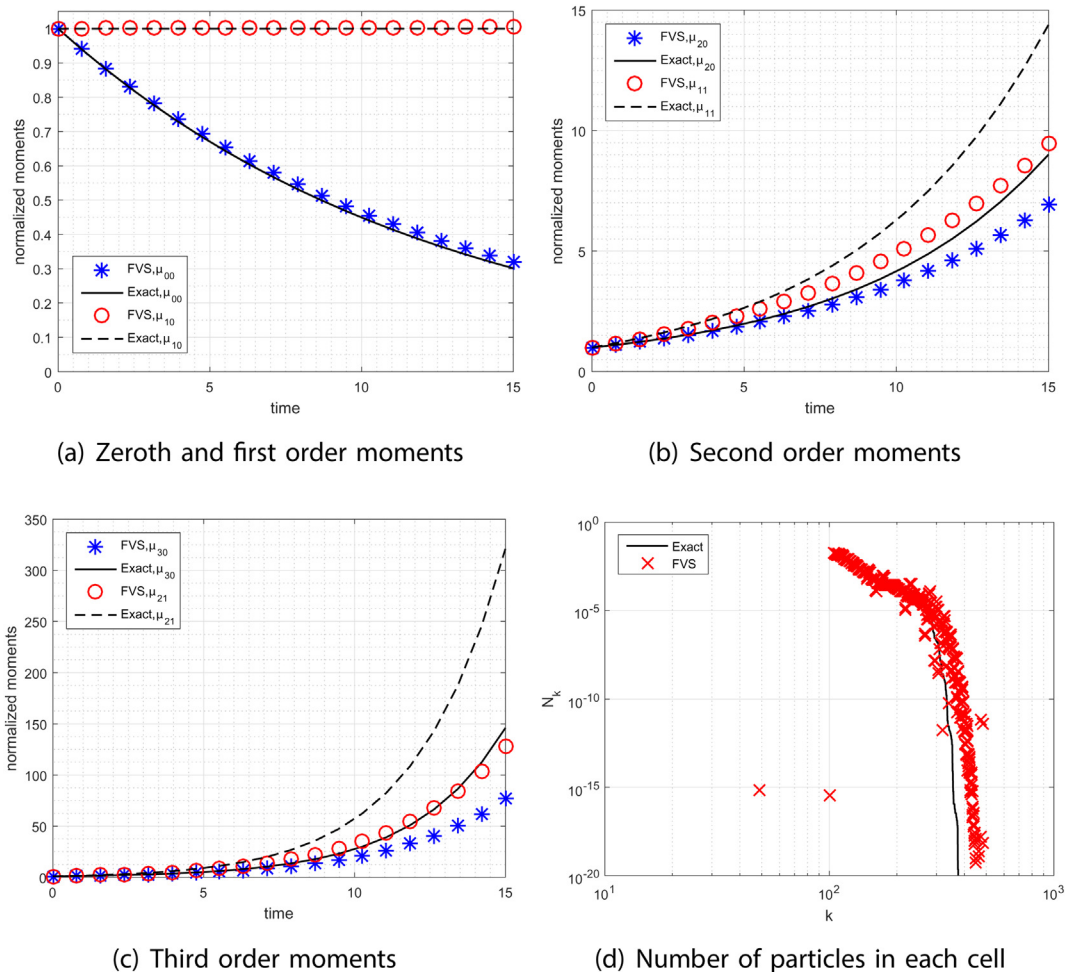
(a) Zeroth and first order moments

(b) Second order moments

(c) Third order moments

(d) Number of particles in each cell

Fig. 10. Different order moments and number density using size-dependent kernel with Type-3 discretization.

mu_{20}) predicted using Type-2 discretization shows less deviation from the analytical moment whereas the moments computed using the other three discretizations show significant deviation (under prediction) from the analytical moment. Likewise, the third order moments (mu_{21} & mu_{30}) also show the similar behavior as second order moments, i.e., the moments predicted by Type-1, Type-3 and Type-4 deviate far from the analytical solutions whereas the third order moments captured using Type-2 show less deviation from the analytical moments.

Analogous to the previous case, for the size-dependent kernel, the number density function obtained numerically for various discretizations are compared graphically (see Figs. 8(d), 9(d), 10(d) and 11(d)). For analyzing the number density functions, the concept of at representation is used. Fig.s reveal that Type-2 discretization approximates the number density function with higher precision as compared to the other discretizations. The quantitative weighted sectional errors in the number density function calculated using the relation (13) are listed in Table 8 for all discretizations. The results exhibit that the errors exist in Type-2 are lesser as compared to Type-1, Type-3 and Type-4 discretizations. In addition, the maximum errors (14) in various order moments obtained using finite volume scheme with four discretizations are also demonstrated in Table 10. The results reveal that the maximum errors computed at the end of time domain are lesser for Type-2 discretization as compared to the other grids. In order to check the accuracy of the finite volume scheme on a refined grid, the quantitative comparison of sectional and maximum errors exist in various order moments is also conducted in Tables 9 and 11. It can be

noticed that these errors reduce to 50% when finite volume scheme is implemented on a refined grid for each discretiztion. However, the Type-2 discretization still outperforms the other discretizations in term of accuracy.

In addition to above, the comparison in terms of computational sense shows that slightly lesser time is taken by finite volume scheme with the Type-2 grid than the other three discretizations. Therefore, it can be concluded that the finite volume scheme with Type-2 discretization approximates the various order moments as well as number density function with higher accuracy and efficiency as compared the other grids. This also illustrates that the solution of the 2D aggregation PBE is highly dependent on the type of discretization chosen to divide the given domain.

5. Conclusions

The finite volume scheme has been applied successfully to four types of non-uniform regular triangular discretizations. Different comparisons of the finite volume scheme with four types of discretizations in terms of maximum as well as sectional weighted errors have been conducted. The qualitative along with the quantitative numerical results computed using the finite volume scheme admit that the results approximated for Type-2 discretization are in better agreement with the analytical results as compared to the results of all other grids. This concludes that the finite volume scheme for solving a 2D aggregation population balance equation is highly dependent on the orientation and
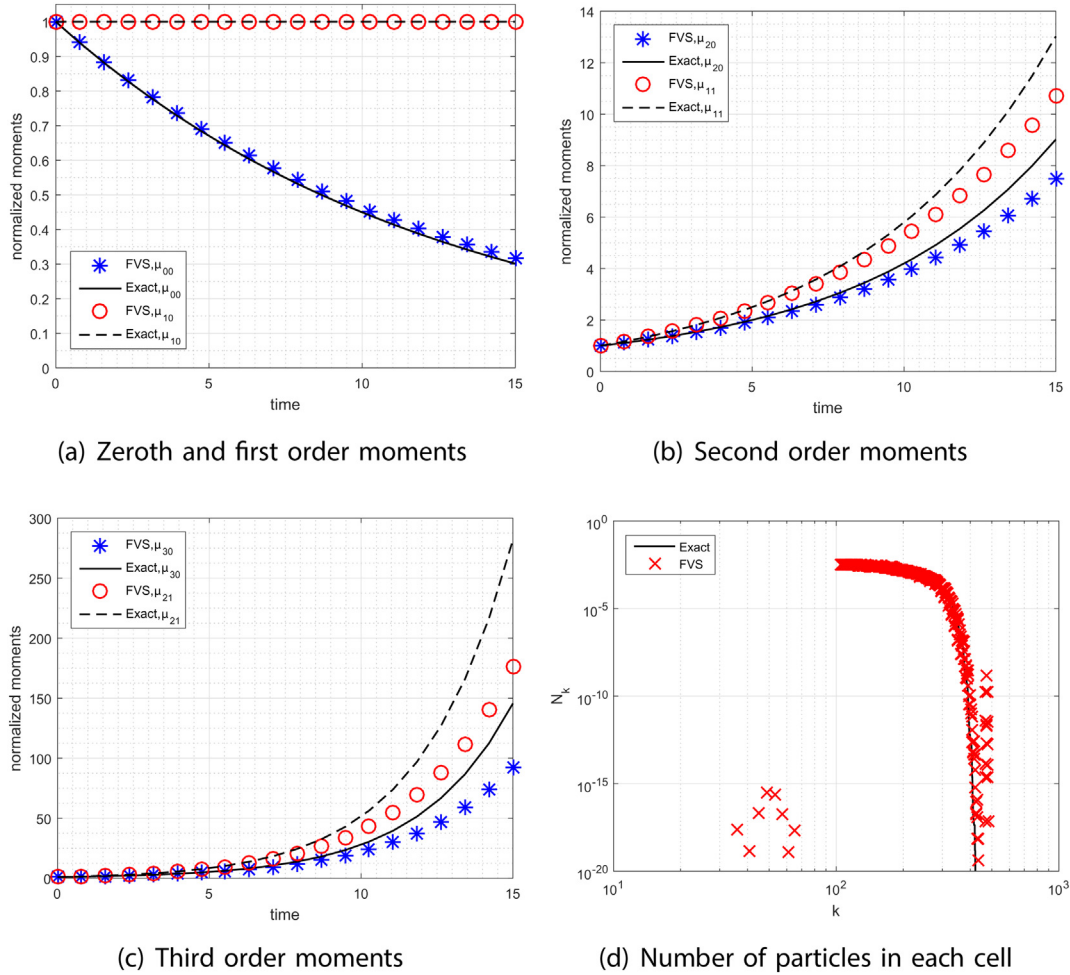
(a) Zeroth and first order moments

(b) Second order moments

(c) Third order moments

(d) Number of particles in each cell

Fig. 11. Different order moments and number density using size-dependent kernel with Type-4 discretization.

directionality of discretization considered for partitioning the given domain.

Appendix A. Appendix

Proposition: The numerical scheme representing by the expression (6) is not mass conserving.

Proof: Multiply the formulation provided in eq. (6) by $(x_i + y_j)$ both side and take sum over all i and j. The left hand side gives the first moment at time t^{k+1} and the right hand side can be simplified as

$$\sum_{i=1}^{I_1}\sum_{j=1}^{I_2} N_{x_i,y_j}^{k+1}\left(x_i + y_j\right)\Delta x_i \Delta y_j = \sum_{i=1}^{I_1}\sum_{j=1}^{I_2} N_{x_i,y_j}^{k}\left(x_i + y_j\right)\Delta x_i \Delta y_j + \Delta t^k T,$$

where T is given by the following expression:

$$T = \sum_{i=1}^{I_1}\sum_{j=1}^{I_2}\left(\sum_{(p,q,r,s)\in\Omega^{i,j}}\left(1 - \frac{1}{2}\delta_{p,q}\delta_{r,s}\right)K_{ijkl}^{k}N_{x_p,y_r}^{k}N_{x_q,y_s}^{k}\Lambda_{p,q,r,s}^{i,j} - \sum_{p=1}^{I_1}\sum_{q=1}^{I_2}K_{ipjq}^{k}N_{x_i,y_j}^{k}N_{x_p,y_q}^{k}\right)$$

(16)

For proving the mass conservation property, it is required to show that $T = 0$ for all times. But, it can be noticed that the two expressions on the right hand side of the above equations are not same. Hence, the mass conservation property does not hold for the formulation (6).

References

[1] N. Ahmed, G. Matthies, L. Tobiska, Finite element methods of an operator splitting applied to population balance equations, J. Comput. Appl. Math. 236 (6) (2011) 1604–1621.

[2] M.M. Attarakih, M. Jaradat, C. Drumm, H.J. Bart, S. Tiwari, V.K. Sharma, J. Kuhnert, A. Klar, A multivariate sectional quadrature method of moments for the solution of the population balance equation, Comput. Aid. Chem. Eng. 28 (2010) 1551–1556.

[3] J. Chakraborty, J. Kumar, M. Singh, A. Mahoney, D. Ramkrishna, Inverse problems in population balances. Determination of aggregation kernel by weighted residuals, Ind. Eng. Chem. Res. 54 (42) (2015) 10530–10538.

[4] J. Chakraborty, S. Kumar, A new framework for solution of multidimensional population balance equations, Chem. Eng. Sci. 62 (15) (2007) 4112–4125.

[5] A. Chaudhury, A. Kapadia, A.V. Prakash, D. Barrasso, R. Ramachandran, An extended cell-average technique for a multi-dimensional population balance of granulation describing aggregation and breakage, Adv. Powder Technol. 24 (6) (2013) 962–971.

[7] S.S. Chauhan, A. Chiney, S. Kumar, On the solution of bivariate population balance equations for aggregation: X–discretization of space for expansion and contraction of computational domain, Chem. Eng. Sci. 70 (2012) 135–145.

[8] C.A. Dorao, H.A. Jakobsen, Numerical calculation of the moments of the population balance equation, J. Comput. Appl. Math. 196 (2) (2006) 619–633.

[9] C.A. Dorao, H.A. Jakobsen, Least-squares spectral method for solving advective population balance problems, J. Comput. Appl. Math. 201 (1) (2007) 247–257.

[10] J. Favero, P. Lage, The dual-quadrature method of generalized moments using automatic integration packages, Comput. Chem. Eng. 38 (2012) 1–10.

[11] J. Fernández-Díaz, G. Gómez-García, Exact solution of smoluchowski's continuous multi-component equation with an additive kernel, Europhys. Lett. 78 (2007), 56002.

[12] L. Forestier-Coste, S. Mancini, A finite volume preserving scheme on nonuniform meshes and for multidimensional coalescence, SIAM J. Sci. Comput. 34 (6) (2012) B840–B860.

[13] F. Gelbard, J. Seinfeld, Simulation of multicomponent aerosol dynamics, J. Colloid Interface Sci. 78 (2) (1980) 485–501.

[14] W. Hackbusch, Approximation of coalescence integrals in population balance models with local mass conservation, Numer. Math. 106 (4) (2007) 627–657.

[15] M. Hussain, J. Kumar, M. Peglow, E. Tsotsas, On two-compartment population balance modeling of spray fluidized bed agglomeration, Comput. Chem. Eng. 61 (2014) 185–202.
[16] S.M. Iveson, Limitations of one-dimensional population balance models of wet granulation processes, Powder Technol. 124 (3) (2002) 219–229.
[17] G. Kaur, J. Kumar, S. Heinrich, A weighted finite volume scheme for multivariate aggregation population balance equation, Comput. Chem. Eng. 101 (2017) 1–10.
[18] Y. Kim, J. Seinfeld, Simulation of multicomponent aerosol condensation by the moving sectional method, J. Colloid Interface Sci. 135 (1) (1990) 185–199.
[19] A. Kumar, J. Vercruysse, V. Vanhoorne, M. Toiviainen, P.-E. Panouillot, M. Juuti, C. Vervaet, J.P. Remon, K.V. Gernaey, T. De Beer, et al., Conceptual framework for model-based analysis of residence time distribution in twin-screw granulation, Eur. J. Pharm. Sci. 71 (2015) 25–34.
[20] J. Kumar, G. Kaur, E. Tsotsas, An accurate and efficient discrete formulation of aggregation population balance equation, Kin. Related Models 9 (2) (2016).
[21] J. Kumar, M. Peglow, G. Warnecke, S. Heinrich, The cell average technique for solving multi-dimensional aggregation population balance equations, Comput. Chem. Eng. 32 (8) (2008) 1810–1830.
[22] J. Kumar, G. Warnecke, Convergence analysis of sectional methods for solving breakage population balance equations-I: the fixed pivot technique, Numer. Math. 111 (1) (2008) 81–108.
[23] J. Kumar, G. Warnecke, Convergence analysis of sectional methods for solving breakage population balance equations-II: the cell average technique, Numer. Math. 110 (4) (2008) 539–559.
[24] J. Kumar, G. Warnecke, M. Peglow, S. Heinrich, Comparison of numerical methods for solving population balance equations incorporating aggregation and breakage, Powder Technol. 189 (2) (2009) 218–229.
[25] S. Kumar, D. Ramkrishna, A general discretization technique for solving population balance equations involving bivariate distributions, AIChE Annual Meeting, Miami Beach, FL, USA, November, Vol. 12, 1995, p. 17.
[26] D.L. Marchisio, R.O. Fox, Solution of population balance equations using the direct quadrature method of moments, J. Aerosol Sci. 36 (1) (2005) 43–73.
[27] G. Marshall, Monte Carlo methods for the solution of nonlinear partial differential equations, Comput. Phys. Commun. 56 (1) (1989) 51–61.
[28] T. Matsoukas, T. Kim, K. Lee, Bicomponent aggregation with composition-dependent rates and the approach to well-mixed state, Chem. Eng. Sci. 64 (4) (2009) 787–799.
[29] T. Matsoukas, K. Lee, T. Kim, Mixing of components in two-component aggregation, AICHE J. 52 (9) (2006) 3088–3099.
[30] S. Matveev, V. Stadnichuk, E. Tyrtyshnikov, A. Smirnov, N. Ampilogova, N. Brilliantov, Anderson acceleration method of finding steady-state particle size distribution for a wide class of aggregation–fragmentation models, Comput. Phys. Commun. 224 (2017) 154–163.
[31] M. Nandanwar, S. Kumar, A new discretization of space for the solution of multi-dimensional population balance equations, Chem. Eng. Sci. 63 (8) (2008) 2198–2210.
[32] T.T. Nguyen, F. Laurent, R.O. Fox, M. Massot, Solution of population balance equations in applications with fine particles: mathematical modeling and numerical schemes, J. Comput. Phys. 325 (2016) 129–156.
[33] S. Qamar, G. Warnecke, Solving population balance equations for two-component aggregation by a finite volume scheme, Chem. Eng. Sci. 62 (3) (2007) 679–693.
[34] S. Rigopoulos, A. Jones, Finite-element scheme for solution of the dynamic population balance equation, AICHE J. 49 (5) (2003) 1127–1139.
[35] M. Singh, D. Ghosh, J. Kumar, A comparative study of different discretizations for solving bivariate aggregation population balance equation, Appl. Math. Comput. 234 (2014) 434–451.
[36] M. Singh, G. Kaur, H.-J. Bart, Approximation of Multidimensional Pure Aggregation Population Balance Equation on a Structured Triangular Mesh: A Finite Volume Approach (Communicated), 2018.
[37] M. Singh, G. Kaur, J. Kumar, D.B. Thomas, I. Nopens, A comparative study of numerical approximations for solving smoluchowski coagulation equation, Braz. J. Chem. Eng. 35 (3) (2017).
[38] M. Singh, G. Kaur, D.B. Thomas, I. Nopens, Solution of bivariate aggregation population balance equation: a comparative study, React. Kinet. Mech. Catal. 123 (2) (2018) 385–401.
[39] M. Singh, J. Kumar, A. Bück, E. Tsotsas, A volume-consistent discrete formulation of aggregation population balance equations, Math. Methods Appl. Sci. 39 (9) (2015) 2275–2286.
[40] M. Singh, J. Kumar, A. Bück, E. Tsotsas, An improved and efficient finite volume scheme for bivariate aggregation population balance equation, J. Comput. Appl. Math. 308 (2016) 83–97.
[41] H. Vale, T. McKenna, Solution of the population balance equation for two-component aggregation by an extended fixed pivot technique, Ind. Eng. Chem. Res. 44 (20) (2005) 7885–7891.
[42] S. Wu, E.K. Yapp, J. Akroyd, S. Mosbach, R. Xu, W. Yang, M. Kraft, Extension of moment projection method to the fragmentation process, J. Comput. Phys. 335 (2017) 516–534.
[43] S. Wu, E.K. Yapp, J. Akroyd, S. Mosbach, R. Xu, W. Yang, M. Kraft, A moment projection method for population balance dynamics with a shrinkage term, J. Comput. Phys. 330 (2017) 960–980.

Nomenclature

Symbol: Description
n: Number distribution (density) function
K: Aggregation kernel
$K_0(t)$: Aggregation frequency
$N_p^{ana}(t^k)$: Analytical (Exact) value of number of particles in the cell p at time t^k
$N_p^{num}(t^k)$: Numerical value of number of particles in the cell p at time t^k
μ: Moments of number density function
I: Total number of cells
I_{agg}: Degree of aggregation
λ: Restricted domain
x, y: Particle properties in terms of size (volume)
Λ: Weight for the finite volume scheme
ψ: Weighted sectional errors in number density function
η: Maximum errors in moments

Abbreviations

PBE: Population balance equation
FVS: Finite volume scheme
CAT: Cell average technique
DOA: Degree of aggregation